ARTICLES

Using $^{87}Sr/^{86}Sr$ Ratios to Date Fossil Methane Seep Deposits: Methodological Requirements and an Example from the Great Valley Group, California

Steffen Kiel,[1,][*] Christian Hansen,[2,3] Kai N. Nitzsche,[2,4] and Bent T. Hansen[2]

1. Georg-August University Göttingen, Geoscience Center, Geobiology Group, Goldschmidtstraße 3, 37077 Göttingen, Germany; 2. Georg-August University Göttingen, Geoscience Center, Department of Isotope Geology, Goldschmidtstraße 3, 37077 Göttingen, Germany; 3. University of Bremen, Geoscience Department, Klagenfurter Straße, 28359 Bremen, Germany; 4. Leibniz Center for Agricultural Landscape Research (ZALF), Institute for Landscape Biogeochemistry, Eberswalderstraße 84, 15374 Müncheberg, Germany

ABSTRACT

Methane seep carbonates preserve information about the history of methane seepage and of the fauna inhabiting these ecosystems. For this information to be useful, a reliable determination of the carbonates' stratigraphic ages is required, but this is not always available. Here we investigate the using strontium isotope stratigraphy to date fossil methane seep carbonates via detailed petrographic and geochemical investigation of the different carbonate phases in biostratigraphically well-dated seep carbonates of Paleozoic, Mesozoic, and Cenozoic age. The best results are obtained from banded, botryoidal rim cements from carbonate phases showing a weak or no cathodoluminescence signal, an oxygen isotope signature close to that of seawater, and the lowest Mn concentrations. We then applied the method to a presumably late Jurassic seep carbonate from the Great Valley Group in California. Strontium isotope ratios of the least diagenetically altered carbonate phases indicate a Tithonian (late Jurassic) age for this seep site, which is in conflict with a recent study that suggested the absence of Jurassic strata from the Great Valley Group.

Introduction

Marine methane seeps are places where methane-rich fluids from the subsurface reach the seafloor. Here most of the methane is oxidized by a consortium of microorganisms using seawater sulfate as electron donor (Boetius et al. 2000), which often results in the precipitation of carbonate due to a local increase in pH (Peckmann and Thiel 2004). This makes methane seeps and the associated carbonates an important sink of the greenhouse gas methane. Interesting from a biological perspective is that methane seeps are inhabited by an unusual and highly specialized fauna similar to that around deep-sea hydrothermal vents, which relies on che-

mosymbiosis for nutrition rather than on photosynthesis (Paull et al. 1984; Levin 2005). Due to its in situ food source, this fauna may have had an independent evolutionary history, unaffected by extinction events caused by disruptions of photosynthesis-driven food chains on the surface of the planet. Consequently, the origin of these unique communities and the mechanisms driving their evolution are the matter of a controversial debate (Newman 1985; Vrijenhoek 2013).

Fossil methane-seep deposits provide important insights into the biological and geochemical evolution of these systems. Biomarkers (molecular fossils) preserved in methane-seep carbonates allow tracing of microbial methane oxidation back into Carboniferous time (Birgel et al. 2008) and reconstruction of fluid flow intensities in the geo-

logic past (Peckmann et al. 2009). The abundance of seep deposits through Earth history suggests a correlation between the extent of seepage on a global scale on the one hand and sea level fluctuations, deepwater temperatures, and seawater sulfate concentration on the other (Kiel 2009; Wortmann and Paytan 2012). Macrofossils preserved in these deposits provide direct evidence for the evolutionary history of these faunas (Campbell and Bottjer 1995; Kiel and Little 2006; Kiel et al. 2012; Little and Vrijenhoek 2003). Such studies require that the stratigraphic age of the methane-seep deposits in question be well established, but that is not always the case. Problems arise when the surrounding sediments do not contain index fossils (e.g., California: Campbell and Bottjer 1993; or Barbados: Gill et al. 2005), when the contact between carbonate and surrounding sediment is not clear (e.g., Peru: Olsson 1931; Campbell 2006), when the seep limestones are retrieved from olisthostromes (e.g., northern Italy: Berti et al. 1994), or when fossils found in museum collections lack sufficient documentation (e.g., Colombia, Cuba: Kiel and Peckmann 2007).

Here we investigate to which extent $^{87}Sr/^{86}Sr$ ratios in seep carbonates can be used for dating. These ratios have varied through Earth's history due to changing inputs from sources with different $^{87}Sr/^{86}Sr$ ratios, that is, weathering of granitic basement rocks and seafloor volcanism, among others, and they are recorded in marine carbonates (Faure and Mensing 2004). Several thousand measurements of samples with known biostratigraphic ages have been compiled into a Phanerozoic Sr isotope curve that can be used to infer the age of a marine carbonate sample based on its $^{87}Sr/^{86}Sr$ ratio, at least within certain limits (McArthur et al. 2012). The approach works best when the sample in question is from a geologic time interval in which the Sr isotope curve exhibits a directional change so that an $^{87}Sr/^{86}Sr$ ratio can unequivocally be assigned to a geologic age (McArthur et al. 2012). The approach also requires that the sample (i) has indeed recorded the original $^{87}Sr/^{86}Sr$ ratio of seawater, and (ii) is not diagenetically altered (Faure and Mensing 2004).

At methane seeps, the seeping fluids sometimes carry a different isotopic signature than the ambient seawater, as for example in the northern Gulf of Mexico where fluids are enriched in lighter "Mesozoic" strontium (Paull et al. 1991). However, the seep carbonates appear to "inherit" almost entirely the $^{87}Sr/^{86}Sr$ ratio of the ambient seawater (Aharon et al. 1997; Peckmann et al. 2001). Fossil seep carbonates consist of a complex mixture of different carbonate phases, some of which may be diagenetically altered (e.g., Greinert et al. 2001; Peckmann et al. 2001; Campbell et al. 2002). First we established which carbonate phases are best suited for Sr isotope dating, by characterizing the various carbonate phases geochemically petrographically and then comparing ages derived from the $^{87}Sr/^{86}Sr$ ratios of these phases (using the LOWESS 5.0 curve of McArthur et al. 2012) to the known biostratigraphic age of the seep deposits. For this purpose, we investigated three biostratigraphically well-dated seep deposits of Paleozoic, Mesozoic, and Cenozoic age. Then we applied Sr isotope dating to a presumably late Jurassic seep deposit from the late Mesozoic Great Valley Group in California. The existence of Jurassic strata within the Great Valley Group has recently been questioned (Surpless et al. 2006), and thus, dating of a supposedly late Jurassic seep deposit from this area could shed new light on this question.

Methods

Thin sections of 50–60 μm thickness were studied using a Zeiss Axioplan optical stereomicroscope; for cathodoluminescence (CL), we used a CITL CCL 8200 Mk 3A cold cathode device. Samples for carbon, oxygen, and strontium isotope analyses and for X-ray diffraction (XRD) analysis were extracted from the polished surfaces of the counterparts of the thin sections using a handheld microdrill. For C and O isotope analyses, carbonate powders were reacted with 100% phosphoric acid at 75°C using a Finnigan Kiel IV Carbonate Device attached to a Finnigan DELTA V PLUS mass spectrometer. All values are reported (per mil) relative to the Vienna Pee Dee belemnite standard (V-PDB) by assigning a $\delta^{13}C$ value of +1.95‰ and a $\delta^{18}O$ value of −2.20‰ to NBS19. Reproducibility was checked by replicate analysis of laboratory standards and was better than ±0.05‰. XRD analyses were done on a Philips PW 1800 diffractometer using $Cu_{K\alpha 1}$ radiation and an automatic divergence plate at 45 kV beam energy and 30 mA beam current.

Trace element analysis was done by laser ablation–inductively coupled plasma-mass spectroscopy (LA-ICP-MS), using a PerkinElmer SCIEX ELAN DCR II mass spectrometer coupled to a Lambda Physik Compex 110 argon-fluoride-laser with a wavelength of 193 nm. A low-volume sample chamber with a size of 5 cm × 3 cm × 0.5 cm (L × W × H) was fixed onto the samples and flushed with argon gas. The laser was moved over the sample at ~40 μm/s with a spot size of 120 μm; external standard was NBS 610.

Samples were analyzed for $^{87}Sr/^{86}Sr$ isotopic composition using standard cation-exchange procedures for the chemical separation, and they were measured on a ThermoFinnigan Triton mass spectrometer at the Department of Isotope Geology, Geoscience Center, University of Göttingen. Samples were typically treated with hydrochloric acid during the chemical decomposition; when samples had to be treated with hydrofluoric acid due to smaller silicate impurities within the carbonate, it is noted in the tables. Before digestion, samples were mixed with a tracer solution enriched in ^{87}Rb and ^{84}Sr. Concentrations were calculated using the isotpic dilution–thermal ionization mass spectrometry; if no concentrations are quoted, the measurements were made on unspiked samples. During this work, a value of 0.710272 ± 0.000039 (2δ) for the NBS 987 ($n = 8$) was observed. Instrumental mass bias was corrected with $^{88}Sr/^{86}Sr$ of 0.1194 using exponential law. Mass bias correction for Rb measurements was achieved via repeated analyses of SRM 984 yielding an $^{85}Rb/^{87}Rb$ of 2.6014 ± 42 ($n = 12$). Sample measurements were performed under the same conditions and corrected with the factor derived from the standard measurements.

$^{87}Sr/^{86}Sr$ ratios given as "$^{87}Sr/^{86}Sr(corr)^*$" in tables 1–4 are corrected for blank, mass fractionation, and Rb decay with an age corresponding to the biostratigraphic age of the respective carbonates reported in the locality descriptions (the maximum Rb correction was -0.0004 of the measured ratios). After these corrections, the $^{87}Sr/^{86}Sr$ ratios were adjusted to 0.710248 for the NBS 987, which is the normalization ratio for the LOWESS curve and lookup table, version 5.0, of McArthur et al. (2012); the values for the best fit and for the upper and lower 95% confidence intervals are given in tables 1–4. Absolute ages were translated into geologic stages based on Gradstein et al. (2012).

Test Cases

Bear River (Cenozoic, Late Eocene). *Locality Description.* The Bear River seep deposit is located in southwestern Washington State, in an abandoned quarry on the south side of Bear River (Goedert and Squires 1990; coordinates: 46°19.943′N, 123°55.964′W). The siltstone enclosing the carbonate body contains the calcareous nannofossil *Isthmolithus recurvus*, characteristic for the late Eocene CP15b zone of Okada and Bukry (1980), which corresponds to an absolute age of ca. 34 m.yr. in the Gradstein et al. (2012) timescale.

Carbonate Characterization. The limestone is volumetrically dominated by a fine-grained micritic matrix which macroscopically is either dark gray or beige-greenish. Fossils including mytilid and vesicomyid bivalves and the siliceous sponge *Aphrocallistes* are frequently embedded in this matrix (fig. 1A). The numerous vugs and cavities reaching several centimeters in diameter are lined with botryoidal and/or banded rim cements (fig. 1B). The center of the cavities may be filled with either clotted micrite or partially translucent sparry calcite. A complex history of carbonate precipitation and dissolution is indicated by frequent dissolution fronts marked by thin layers of pyrite. XRD analyses show that matrix and rim cements are mainly calcitic; only the clotted micrite includes minor amounts of dolomite, Mg-calcite, and ankerite. All carbonate phases showed little or no CL signal. The Sr content of the carbonate phases is around 2000 ppm and shows no systematic variation. Likewise, the different carbonate phases show no significant differences among their carbon and oxygen isotope signatures, with $\delta^{13}C$ values ranging from $-38.6‰$ to $-32.6‰$ and corresponding $\delta^{18}O$ values from $-9.2‰$ to $-5.2‰$. The Rb content varied systematically: matrix and cavity micrites had consistently more Rb (2.71 to 19.65 ppm) than the rim cement (0.51 to 0.8 ppm) and the sparry calcite (0.04 to 0.56). The Mn content was generally low, ranging from 100 ppm in the sparry calcite to 266 in the clotted micrite, and Fe concentrations varied from ~4000 in the sparry calcite to >18,000 ppm in the clotted micrite; see table 1 for a summary of the data.

Sr Isotope Dating. $^{87}Sr/^{86}Sr$ ratios range from 0.707810 to 0.708080 with one outlier that was presumably contaminated by quartz (0.707583) and therefore not taken into further consideration (table 1). The calculated Sr isotope ages range from to 26.85 to 34.25 Ma, with a median of 33.33 Ma, which is close to the biostratigraphic age of ca. 34 Ma. The two best Sr isotope ages, although by a thin margin, are derived from rim cements. The carbonate phase with the least reliable Sr isotope ratios included dolomite and ankerite, while in all other carbonate phases, any mineral but calcite was below the detection limit of the X-ray diffractometer. There were no mixing lines among and no systematic correlation or covariation of the $^{87}Sr/^{86}Sr$ ratios with Sr, Rb, Mn, and Fe concentrations or C and O isotope ratios.

Remarks. Two Sr isotope ages match the biostratigraphic age of the Bear River seep deposit, most others are only slightly younger (1 to 2 Ma). This is a remarkably small deviation considering that most carbonate phases had $\delta^{18}O$ values of

Table 1. Summary of Results for the Bear River Seep Carbonate; Mn and Fe Concentrations from Laser Ablation–ICP-MS Measurements; Sr and Rb Concentrations Measured Using Isotope Dissolution

Carbonate type	Mineralogy	Mn (ppm)	Fe (ppm)	$\delta^{13}C_{PDB}$ (‰)	$\delta^{18}O_{PDB}$ (‰)	$^{87}Sr/^{86}Sr$ (measured)	Uncertainty (2σ)	Sr (µg/g)	Rb (µg/g)	$^{87}Sr/^{86}Sr$ (corr)*	Mean age (Ma)	Lower age (Ma)	Upper age (Ma)
Beige micritic matrix	Cal	173	5452										
1				−37.6	−7.7	.707873	.000015	1776	6.47	.7078451	32.92	32.52	33.32
2				−37.6	−7.8	.707877	.000015	1820	9.12	.7078471	32.89	32.46	33.28
3				−36.9	−8.1	.707883	.000017	1876	7.93[a]	.7078531	32.79	32.30	33.19
Gray micritic matrix	Cal	166	5425										
1				−38.2	−7.7	.707882	.000012	1816	8.48	.7078521	32.81	32.42	33.14
2				−38.1	−7.9	.707892	.000012	1425	7.43	.7078611	32.66	32.21	32.99
3				−37.8	−7.5	.707915	.000016	1633	10.34	.7078831	32.20	31.62	32.70
Banded/botryoidal cement	Cal, Py	221	15,251										
1				−38.1	−7.3	.707833	.000016	2360	.64	.7078101	33.53	33.11	33.95
2				−38.6	−7.9	.708104	.000041	2162	.80	.7080800	26.65	25.04	28.17
3				−37.8	−5.9	.707840	.000014	2570	.51	.7078171	33.40	33.03	33.78
Clotted micrite	Cal, Dol, Mg-Cal, Ank	266	18,523										
1				−38.4	−5.3	.708040	.000013	1436	19.65	.7079981	28.97	28.45	29.53
2				−38.6	−5.2	.707959	.000014	1979	9.85	.7079291	30.92	30.23	31.64
3				−35.0	−5.3	.707973	.000016	2570	11.73	.7079441	30.47	29.70	31.22
Sparry calcite	Cal	100	4018										
1[b]				−32.6	−9.2	.707606	.000019	539	.09	.7075831	ND[c]	ND[c]	ND[c]
2				−37.4	−7.6	.707867	.000019	2179	.04	.7078441	32.94	32.44	33.39
3				−36.8	−7.7	.707898	.000059	2232	.56	.7078751	32.37	30.52	33.56

Note.   Ank = ankerite, Cal = calcite, and Dol = dolomite.

[a] Missing Rb measurement; the value is the mean of the two other measurements from this carbonate phase.

[b] Samples treated with hydrofluoric acid

[c] Not determined (ND), value outside the LOWESS curve, contamination with quartz suspected

Table 2. Summary of Results for the Eagle Creek Seep Carbonate

Carbonate type	Mineralogy	Mn (ppm)	Fe (ppm)	$\delta^{13}C_{PDB}$ (‰)	$\delta^{18}O_{PDB}$ (‰)	$^{87}Sr/^{86}Sr$ (measured)	Uncertainty (2σ)	Sr (μg/g)	Rb (μg/g)	$^{87}Sr/^{86}Sr$ (corr)*	Mean age (Ma)	Lower age (Ma)	Upper age (Ma)
Micritic matrix	Cal, Mg-Cal, Py, Ms, Ilt, Qz	1414	13,499										
1				−42.1	−2.9	.707152	.000010	431	17.58	.706919	ND[a]	ND[a]	ND[a]
2				−45.4	.0	.707519	.000013	514	20.36	.707291	119.19	118.17	120.47
3				−46.3	.0	.707512	.000012	508	18.22	.707304	120.19	119.02	121.30
Banded/botryoidal cement	Cal	172	370										
1				−35.0	−4.5	.707198	.000009	1100	.03	.707174	ND[a]	ND[a]	ND[a]
2				−40.5	−3.0	.707256	.000017	1020	.05	.707232	115.82	114.38	117.05
3				−34.6	−6.8	.706958	.000011	768	.08	.706934	ND[a]	ND[a]	ND[a]
Yellow calcite	Cal	606	1385										
1				−27.3	−5.0	.706563	.000014	727	.04	.70654			
2				−20.7	−7.6	.706362	.000010	526	.51	.706334			
3				−35.3	−5.5	.706623	.000016	841	.48	.706597			
Sparry calcite[b]	Cal, Brt	4750	5341										
1				−22.7	−13.7	.705546	.000016	647	ND[c]	.705523			
2				−23.9	−12.1	.705576	.000018	383	ND[c]	.705553			
3				−18.9	−13.8	.705569	.000018	397	.09	.705545			
Granular calcite	Cal	5606	2491										
1				−13.0	−10.4	.705699	.000013	413	4.6	.705619			
2				−10.7	−10.8	.705689	.000030	461	3.92	.705622			
3				−21.1	−8.2	.706264	.000018	619	4.32	.706205			

Note. Brt = barite, Ilt = illite, Ms = muscovite, and Qz = quartz; for other abbreviations, see table 1.
[a] Not determined (ND), value outside the LOWESS curve for the Mesozoic.
[b] Samples treated with hydrofluoric acid.
[c] Missing Rb measurement; value inferred from a single measurement from this carbonate phase.

Table 3. Summary of Results for the Tentes Mound Seep Carbonate

Carbonate type	Mineralogy	Mn (ppm)	Fe (ppm)	$\delta^{13}C_{PDB}$ (‰)	$\delta^{18}O_{PDB}$ (‰)	$^{87}Sr/^{86}Sr$ (measured)	Uncertainty (2σ)	Sr (µg/g)	Rb (µg/g)	$^{87}Sr/^{86}Sr$ (corr)*	Mean age (Ma)	Lower age (Ma)	Upper age (Ma)
Brown matrix micrite	Cal, Dol	985	22,779										
1				−12.7	−10.9	.709308	.000018	957	32.42	.708847			
2[a]				2.3	−2.9	.709483	.000020	484	33.41	.708568			
3[a]				−16.5	−11.7	.709398	.000065	1198	45.24	.708887			
Gray matrix micrite	Cal, Dol	439	6474										
1				−18.7	−15.7	.710161	.000008	855	25.76	.709749			
2[a]				−23.8	−15.6	.709349	.000015	1750	26.82	.709128			
3[a]				−20.4	−15.6	.709913	.000020	1496	23.73	.709685			
Clotted micrite	Cal, Mg-cal	238	1908										
1				−35.9	−14.8	.708418	.000027	3954	3.05	.708385			
2[a]				−40.5	−9.1	.708369	.000021	5904	2.77	.70834			
3[a]				−13.0	−15.6	.708985	.000019	1402	7.13	.708897			
Banded-botryoidal cement	Cal	47	395										
1				−41.8	−1.9	.708257	.000020	5855	.01	.708234	314.75	310.90	317.00
2				−43.1	−.8	.708282	.000013	6549	.02	.708259	312.40	304.70	314.80
3				−43.4	.3	.708290	.000017	6861	.09	.708267	310.90	305.00	314.50
Dog tooth, drusy mosaic	Cal	1705	2099										
1				−10.8	−13.1	.708673	.000020	1470	.04	.70865			
2				−9.8	−12.1	.708678	.000013	1119	.04	.708655			
3				−15.4	−10.4	.708505	.000017	2285	.05	.708482			
Sparry calcite	Cal	659	1523										
1				−21.8	−13.1	.708981	.000016	1001	.04	.708958			
2				−22.1	−10.7	.708874	.000008	2510	.02	.708851			
3				−18.1	−12.5	.708745	.000021	1242	.03	.708722			

Note. Cal = calcite, Dol = dolomite, Mg-Cal = magnesium-calcite.
Note.
[a] Samples treated with hydrofluoric acid. For abbreviations, see table 1.

Table 4. Results for the Paskenta Seep Carbonate

Sample	$\delta^{13}C_{PDB}$ (‰)	$\delta^{18}O_{PDB}$ (‰)	$^{87}Sr/^{86}Sr$ (corr)[*]	Uncertainty (2σ)	Sr (μg/g)	Rb (μg/g)	Mean age (Ma)	Lower age (Ma)	Upper age (Ma)
1	−40.4	−.2	.707038	.000011	864	.25	151.75	151.85	151.65
2	−35.8	−4.2	.707025	.000006	ND[a]	ND[a]	152.15	152.25	152.05
3	−33.5	−4.6	.706796	.000007	ND[a]	ND[a]			
4	−26.8	−6.1	.706111	.000013	664	6.54			
5	−33.3	−5.0	.706595	.000010	782	.32			
Buchia	−4.4	−6.0	.706757	.000010	ND[a]	ND[a]			

[a] Not determined (ND); see text for explanation.

−8‰ to −5‰, suggesting the influence of meteoric water (assuming a late Eocene seawater $\delta^{18}O$ value of ca. −1‰; cf. Lear et al. 2000) and thereby the potential to alter the Sr isotope ratios. For diagenetic alteration to affect the Sr isotope ratio, pore fluids must have a different Sr isotope ratio than the carbonate (Denison et al. 1994). Thus, a likely explanation for the distribution of Sr isotope ages at the Bear River seep deposit is that diagenesis occurred early and the respective porewater circulated only through late Eocene or early Oligocene sediments and thus did not carry Sr with a very different isotopic signature. Alternatively, because the Sr contents of the studied carbonate phases were quite high, the porewater might simply not have been sufficiently enriched in Sr to induce a significant modification.

Eagle Creek (Mesozoic, Cretaceous, Late Barremian). Locality Description. The Eagle Creek seep deposit is found in northern California, to the south of Ono village and near the confluence of Eagle Creek and the north fork of Cottonwood Creek (coordinates: 40°27′55.3″N, 122°36′41.1″W), where several seep carbonate blocks are exposed in and along the river bed for about 40 m (Jenkins et al. 2013). Nannoplankton and the ammonite *Shasticrioceras poniente* found in the enclosing Lower Chicabally Mudstone Member indicates a late Barremian age (at least 126 Ma) of this deposit (Fernando et al. 2011; Jenkins et al. 2013).

Carbonate Characterization. Five carbonate phases can be recognized (fig. 2); volumetrically dominant is a dark grayish, fine-grained micritic matrix with few fossil fragments. Vugs and cavities reaching several centimeters in diameter are often filled with several intergrown generations of isopachous, whitish/grayish botryoidal or banded rim cement and isopachous or irregular clusters of yellow calcite. The center of the cavities is filled either by sparitic cements, granular calcite, or peloidal carbonate. XRD indicates that the botryoidal and yellow rim cements and the granular cavity micrite are almost pure calcite, while the sparitic cements also contain barite. The micritic matrix contains

significant amounts of Mg-calcite, pyrite, and mica; however, the abundance of the noncalcite minerals is too low for an exact identification of distinct mica types, and a mixture of muscovite and illite is suggested here. All carbonate phases show a strong CL signal, increasing in intensity toward the center of the cavities; weakest (but still strong compared to the Eocene Bear River seep carbonate) are the banded/botryoidal rim cement and the micritic matrix. The Sr content is low throughout; around 800 to 900 ppm in the yellow calcite and banded/botryoidal rim cements and <500 ppm in the micritic matrix and the cavity-filling granular and sparitic calcite. Carbon and oxygen isotope signatures change consistently from the micritic matrix toward the center of the cavities: the $\delta^{13}C$ values increase from −46.3‰ to −43.1‰ in the micritic matrix to −23.9‰ to −10.7‰ in the sparitic and granular calcitic cavity fills. The corresponding $\delta^{18}O$ values decrease from −2.9‰ to 0‰ in the micritic matrix to −13.8‰ to −8.2‰ in the sparitic and granular calcitic cavity fills. The Rb content is very low in the banded/botryoidal cement (0.03 to 0.08 ppm) and also in the yellow and sparry calcites (0.04 to 0.51 ppm), and it is elevated in the cavity-filling granular calcite (3.92 to 4.6 ppm) and significantly higher in the micritic matrix (17.38 to 20.36 ppm). The Mn content is lowest in the banded botryoidal rim cement (<200 ppm) and highest in the granular calcite (>5000 ppm), and the Fe content is also lowest in the banded botryoidal rim cement (370 ppm) but highest in the matrix micrite (>12,000 ppm); see table 2 for a summary of the data.

Sr Isotope Dating. Only three out of 15 measured $^{87}Sr/^{86}Sr$ ratios came near the biostratigraphic age of the Eagle Creek seep deposit (table 2): two from the micritic matrix and one from the banded/botryoidal rim cement. However, the three derived ages range from 116.5 to 120.35 Ma and are thus 6 to 10 m.yr. younger than the biostratigraphic age of this deposit. It is noteworthy that the two carbonate phases that produced the "best" Sr isotope ages showed the weakest CL signal in this sample.
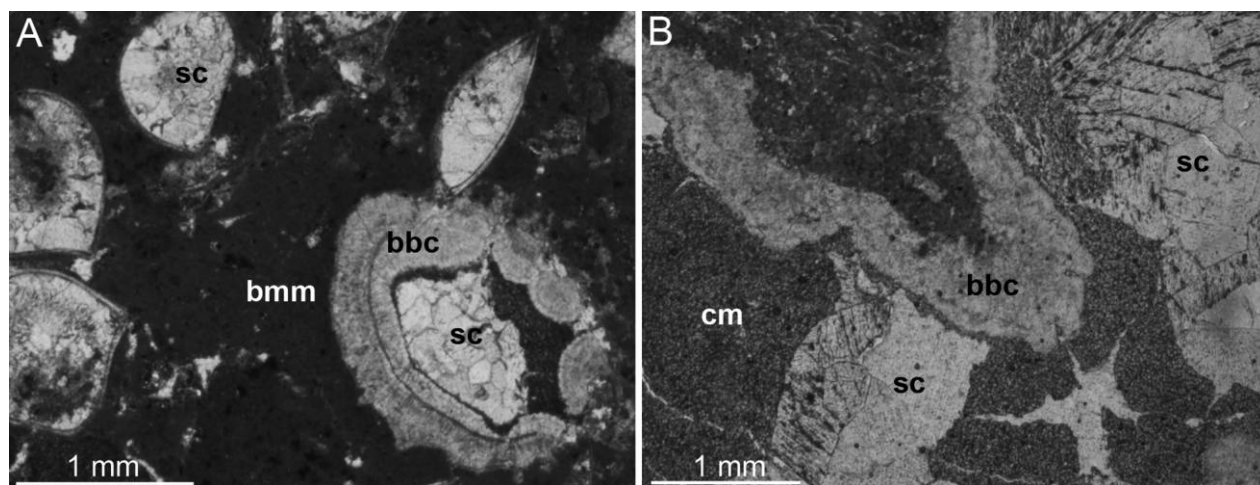
Figure 1. Thin-section images showing the complex carbonate phases of the Bear River seep carbonate. *A*, Void filled with rim cement and sparry calcite in the center, and several cross sections of mussels filled with sparry calcite only. *B*, Large void filled with clotted micrite and sparry calcite. bbc = banded botryoidal cement, bmm = beige matrix micrite, cm = clotted micrite, and sc = sparry calcite. A color version of this figure is available online.

Furthermore, the carbon and oxygen isotope signatures on the one hand and the strontium isotope signatures on the other clearly show mixing lines (fig. 3): the lower the $\delta^{13}C$ values and the higher the $\delta^{18}O$ values, then the higher the respective $^{87}Sr/^{86}Sr$ ratios, which are thereby closer to the ratios that provide the most reliable age estimate. As in the case of the Bear River seep deposit, there is no systematic correlation or covariation of the $^{87}Sr/^{86}Sr$ ratios with Sr and Rb concentration and hence with the reliability of the Sr isotope dating.

Remarks. Two observations indicate that the late diagenetic fluids at the Eagle Creek deposit were depleted in ^{87}Sr: first, the mixing lines between the Sr and O isotope ratios from early to late diagenetic carbonate phases, and second, the only marginal scatter in the $^{87}Sr/^{86}Sr$ ratios among the late diagenetic sparry calcite, while earlier diagenetic carbonate phases show a wide scatter (fig. 3). Furthermore, the two "best" Sr isotope ages were sampled from micritic matrix with no obvious microfractures in the vicinity, while the third, slightly more ^{87}Sr-depleted sample showed several microfractures. Thus, it seems possible that ^{87}Sr-depleted, late diagenetic fluids infiltrated the entire seep carbonate along such microcracks, thereby causing the relatively poor correlation between the biostratigraphic and the Sr isotope ages as well as the wide scatter of $^{87}Sr/^{86}Sr$ ratios in the early diagenetic carbonate phases. A likely cause for the ^{87}Sr depletion of the late diagenetic fluids is its contact with the serpentinites a few kilometers to the west of Eagle Creek (Murphy et al. 1969); serpentinites are al-

tered oceanic crust and are generally strongly depleted in ^{87}Sr (Veizer 1989).

Tentes Mound (Paleozoic, Carboniferous, Late Bashkirian). *Locality Description.* The Tentes Mound is located near the Tentes Pass in the French Pyrenees (coordinates: 42°42.856′N, 0°03.343′W) about 45 km south of Lourdes. Carbonate blocks that crop out over an area of ca. 5 m × 15 m were deposited on top of the dark, laminated Calcaires de l'Iraty and are overlain by shales and sandstones of the Kulm Flysch; conodonts extracted from the limestone indicate a late Bashkirian age (Buggisch and Krumm 2005), which corresponds to an absolute age of ca. 319 to 315 Ma in the Gradstein et al. (2012) timescale.

Carbonate Characterization. Three main facies occur in the Tentes Mound: (1) nodular micrite with large and abundant cavities, (2) homogenous micrite with elongate burrows, and (3) heterogeneous peloidal and fossiliferous micrite; the latter facies was not investigated here. Seven carbonate phases can be recognized (fig. 4); six of them were investigated in this study. The matrix of facies 1 consists mainly of clotted micrite with intergrown needles, and there are patches of brown homogenous matrix micrite. In facies 2, the volumetrically dominant phase is a light gray matrix micrite. In facies 1, cavities up to several centimeters across are typically rimmed by several generations of banded, whitish, acicular or sometimes botryoidal cements that become more fibrous toward the center of the cavities. This phase is followed by dark gray dog tooth and drusy mosaic cements. The cen-
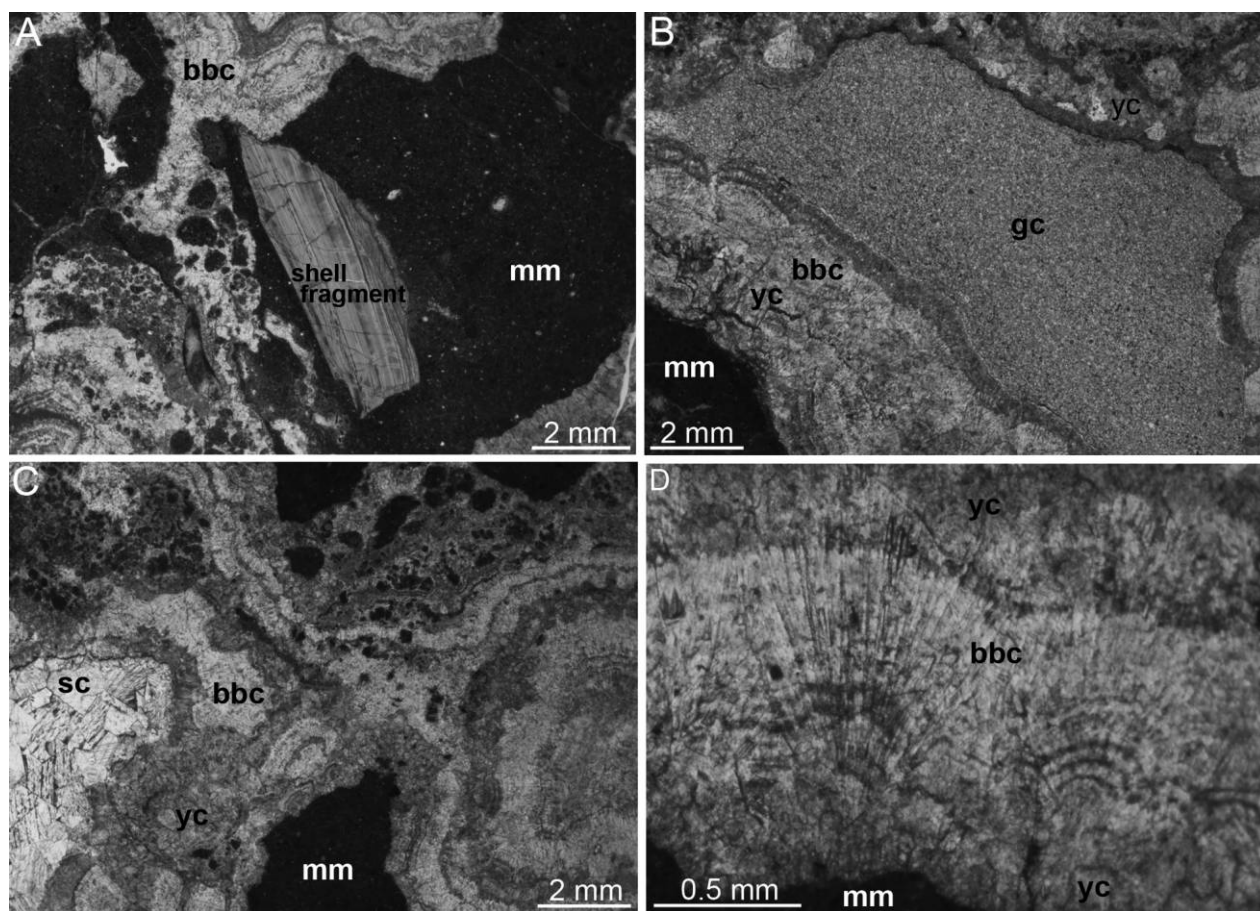
Figure 2. Thin section images of the Eagle Creek seep carbonate showing the occurrence of the sampled carbonate phases. *A*, Matrix micrite with shell fragment and small void fills. *B*, Large void filled with rim cements and granular calcite in the center. *C*, Sequence of carbonate phases filling a cavity in the matrix micrite. *D*, Detail of the banded botryoidal rim cement. bbc = banded botryoidal cement, gc = granular calcite, mm = matrix micrite, sc = sparry calcite, and yc = yellow calcite. A color version of this figure is available online.

ter of the cavities is filled with white sparry calcite. The elongate burrows in facies 2 are lined with rim cement consisting of bladed splays and have sparry calcite in the center. XRD indicates that the matrix micrites contain calcite, Mg-calcite, and dolomite, but the cavity-filling botryoidal, drusy, and sparitic cements are entirely calcitic. The matrix micrites show a very low or no CL signal, as does the banded acicular or botryoidal rim cement. In contrast, a strong CL signal can be seen in the drusy and sparitic cements that fill the cavities. The lowest carbon and highest respective oxygen isotope signatures were measured in the acicular or botryoidal rim cement (δ^{13}C values from −43.4‰ to −41.8‰; δ^{18}O values from −1.9‰ to 0.3‰). The carbon isotope signatures of the remaining carbonate phases are variable, ranging from −40.5‰ in the clotted micrite to 2.3‰ in the brown matrix micrite. The respective oxygen isotope signatures, however, are

rather uniform within and across the carbonate phases, with most values around −15‰ to −10‰. The Sr content is high (>5000 ppm) in the clotted micrite and the banded acicular or botryoidal rim cement and low in the brown matrix micrite (> 500 ppm) and has intermediate concentrations (1000 to 2400 ppm) in the remaining carbonate phases. Rb concentrations are very low in all cavity-filling cements (0.01 to 0.09 ppm), slightly elevated in the clotted micrite (3.05 to 7.13 ppm), and high in the matrix micrites (23.73 to 45.24 ppm). The Mn content is lowest in the banded botryoidal rim cement (<50 ppm) and highest in the drusy mosaic cements (>1700 ppm), and the Fe content is also lowest in the banded botryoidal rim cement (400 ppm) but highest in the brown matrix micrite (>20,000 ppm); see table 3 for a summary of the data.

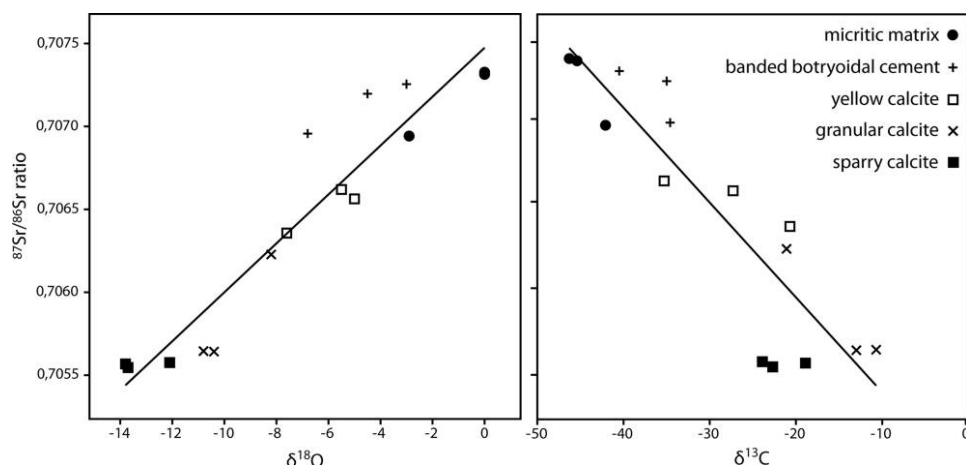*Sr Isotope Dating.* Among the 19 measured ^{87}Sr/^{86}Sr ratios, only three are in general agreement with

Figure 3. Mixing lines of $^{87}Sr/^{86}Sr$ ratio and oxygen (*left*) and carbon (*right*) isotope signatures of the Eagle Creek seep deposit.

the biostratigraphic age of the Tentes Mound, and ages range from 322.65 to 318.50 Ma (mean ages; see table 3). These are from the banded, acicular, or botryoidal rim cement that has the lowest $\delta^{13}C$ signature, the $\delta^{18}O$ signature that is closest to that of seawater among the carbonate phases of the Tentes Mound, and by far the lowest concentrations of Mn and Fe and shows little CL signal. As in the Eagle Creek seep deposit, there is a mixing line between the oxygen and the strontium isotope signatures (fig. 5): the higher the $\delta^{18}O$ values, the lower the $^{87}Sr/^{86}Sr$ ratios and therewith the closer to the biostratigraphic age of the Tentes Mound. There is no such mixing line, however, for the carbon and the strontium isotope signatures. Furthermore, there is a linear correlation between the $^{87}Sr/^{86}Sr$ ratios and the Sr concentration ($r = -0.66$; $P \sim 0.03$; fig. 6): the higher the concentration, the lower the $^{87}Sr/^{86}Sr$ ratios. There is no systematic variation between Mn and Fe concentrations and the Sr isotope ratios in general.

Discussion and Recommendations. Not surprisingly, the Sr isotope ages that were closest to the biostratigraphic ages of the investigated seep deposits are from the least diagenetically altered carbonate phases. The best predictor of a reliable Sr isotope age of a carbonate phase was little or no CL signal: all reliable Sr isotope ages were from phases with little or no CL signal, while phases with a strong CL signal never provided reliable ages. However, there were carbonate phases with little or no CL signal that did not provide reliable ages, in particular Mg-rich calcite and dolomite. For all further parameters, the Eocene Bear Creek seep carbonate behaved different than the Car-

boniferous Tentes Mound and the Cretaceous Eagle Creek seep deposits and will thus be discussed separately. At the latter two localities, oxygen isotope signatures close to those of Early Carboniferous and Early Cretaceous seawater, respectively (cf. Veizer et al. 1999), were another good predictor for reliable Sr isotope ages. These two localities also showed a mixing line among the $\delta^{18}O$ values and the Sr isotope ratios: the further the $\delta^{18}O$ values deviated from that of seawater, the further deviated the Sr isotope ratios from those indicating the biostratigraphic age. This strongly suggests that an increased influence of meteoric water altered Sr isotope ratios. The most reliable Sr isotope ages were from samples with the most negative $\delta^{13}C$ signatures, corresponding to the phases that precipitated under the strongest influence of anaerobic methane oxidation (Peckmann and Thiel 2004). This result supports earlier suggestions that the Sr content of the seeping fluid does not affect the Sr isotope composition of the carbonate (Aharon et al. 1997). Among Paleozoic shelf limestones, Denison et al. (1994) found samples with Mn concentrations of <300 ppm always to yield reliable Sr isotope ratios. Among the carbonate phases tested here, those with the most reliable Sr isotope ratios were those with the lowest Mn concentrations; however, there were phases with Mn concentrations as low as 238 ppm but with inconsistent Sr isotope ratios.

The carbonate phases that provided reliable Sr ages at all three test sites were the banded, botryoidal, or fibrous rim cements. This is remarkable because at least in the cases of the Bear River and the Tentes Mound site, the rim cements were re-
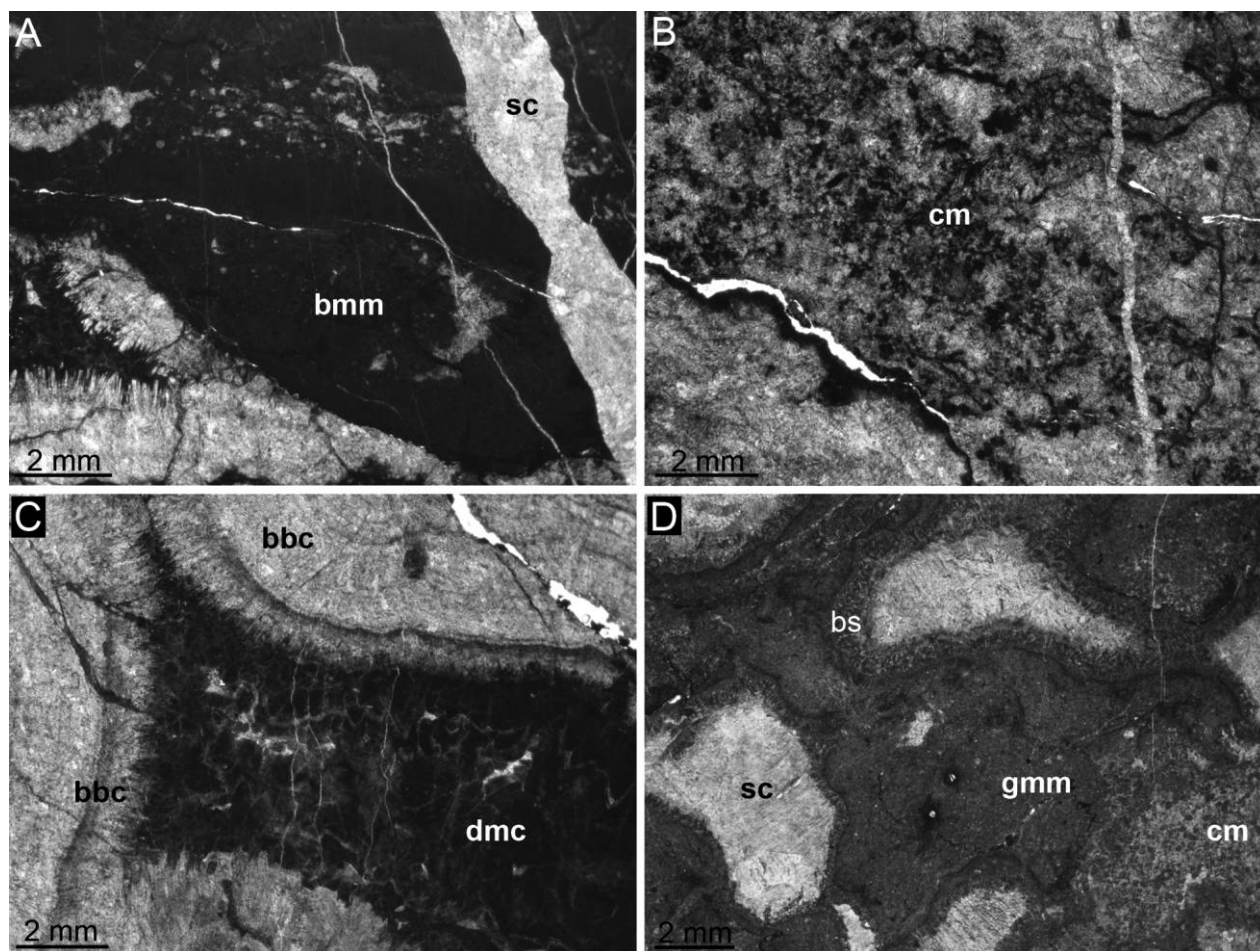
Figure 4. Thin-section images showing the complex carbonate phases of the Tentes Mound seep carbonate. *A*, Matrix micrite, banded and acicular rim cements (*bottom left*) and late diagenetic fracture filling (*right*). *B*, Clotted micrite. *C*, Large void with rim cements and dog tooth and drusy mosaic cement in the center. *D*, Clotted and gray matrix micrite and with cavities filled by sparry calcite and thin rims of bladed splays. bbc = banded botryoidal cement, bs = bladed splays, cm = clotted micrite, dmc = dog tooth and drusy mosaic cement, gmm = gray matrix micrite, and sc = sparry calcite. A color version of this figure is available online.

crystallized from their originally aragonitic mineralogy to calcite, as suggested by their high Sr content. In many cases, rim cements with a low CL signal are directly adjacent to, or even surrounded by, other carbonate phases with a strong CL signal and altered oxygen isotope ratios, suggesting that the rim cements are more resistant against later diagenetic alterations of their chemical composition than the other phases. A plausible explanation is that the rim cements are very dense and thus have little pore space that allows fluids to migrate and later diagenetic carbonate to precipitate. Although the rim cements often provided the most reliable Sr isotope ages, their thin nature makes precise sampling difficult and contamination with material from adjacent carbonate phases is likely.

Some of the outliers from the Bear River and Tentes Mound seeps may result from such contaminations.

An Application: The Great Valley Group, California

Background. The Great Valley Group is a classical example of a forearc basin (Ingersoll 1982; Wright and Wyld 2007) and has long been known for its numerous fossiliferous seep deposits (Campbell et al. 1993, 2002; Kiel et al. 2008). Here we apply Sr isotope dating to a deposit of presumably late Jurassic (Tithonian) age, because the commonly used biostratigraphy on the bivalves *Buchia* and *Aucella* has recently been questioned and doubt was ex-

pressed whether Jurassic strata existed at all in the Great Valley Group (Surpless et al. 2006). The Paskenta seep deposit consists of two elongate, low-relief carbonate lenses 4.8 km northwest of Paskenta by Thomes Camp Road, on a knoll between the road and Digger Creek in Tehama County (coordinates: 39°54′15.42″N, 122°35′49.16″W; Campbell et al. 1993). It occurs within turbidites of the lower middle portion of the Stony Creek Formation (Ingersoll 1978, 1983; Bertucci 1983; Bertucci and Ingersoll 1983) and is dated as middle-upper Tithonian, based on the bivalves *Buchia piochii* and rare *Buchia fischeriana* (Jones et al. 1969).

Five samples were taken from banded fibrous/botryoidal rim cements and one from a moderately well-preserved shell of a *Buchia* bivalve to measure Sr, C, and O isotope ratios; the results are summarized in table 4. The banded fibrous/botryoidal rim cements showed no CL signal. Two samples showed Sr isotope values that are in rough agreement with the suggested biostratigraphic age of the deposit and indicate a basal Tithonian age. These two samples also had the most negative $\delta^{13}C$ signatures, and one had an oxygen isotope value close to that of Jurassic seawater (Veizer et al. 1999). The other samples had $\delta^{18}O$ values as low as −6.1‰, including the *Buchia* shell, indicating the influence of meteoric water, and their Sr isotope ratios would indicate ages beyond the reasonable biostratigraphic frame.

Based on Cretaceous zircons in presumed Jurassic strata from various places within the Great Valley Group, including the area around Paskenta, Surpless et al. (2006) questioned the Jurassic age of these sediments and thereby suggested a much larger thickness of the Cretaceous portion of the
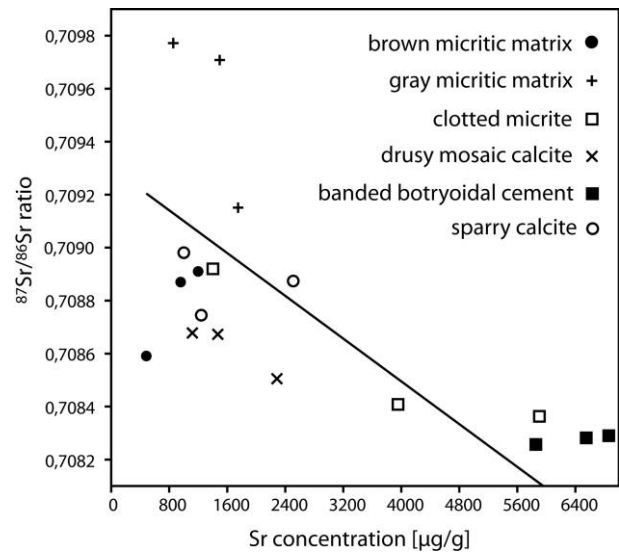

Figure 6. Correlation between $^{87}Sr/^{86}Sr$ ratio and Sr concentration at the Tentes Mound seep deposit.

Great Valley Group, a longer extent of its basal unconformity, and they questioned the validity of the biostratigraphic *Buchia* zonation of these rocks. Our early Tithonian Sr isotope ages of the Paskenta seep deposit conflict with the data presented by Surpless et al. (2006) and suggest that there actually are Jurassic strata in the Great Valley Group, at least in the Paskenta area. An alternative explanation might be that the Paskenta seep carbonates have been reworked into younger (Cretaceous) sediments. But this seems unlikely because of the mode of occurrence of these carbonate bodies, striking parallel (N-S) to the enclosing thin-bedded turbidites (Campbell et al. 1993).
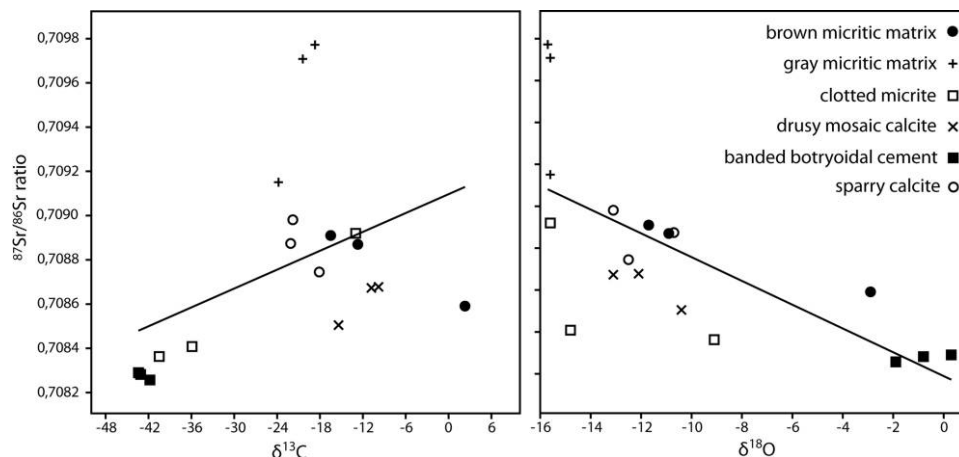

Figure 5. Mixing lines of $^{87}Sr/^{86}Sr$ ratio and carbon (*left*) and oxygen (*right*) isotope signatures of the Tentes Mound seep deposit.

Conclusions

Our results indicate that strontium isotope stratigraphy can be used to better constrain the dating of fossil methane-seep carbonates. When applying this method, we recommend ensuring that only the least diagenetically altered carbonate phases are used, by (1) using only carbonate phases showing little or no CL signal; (2) using only carbonate phases with an O isotope signature close to that of the seawater; (3) using only carbonate phases with the lowest Mn concentration, preferably <300 ppm; (4) targeting early diagenetic rim cements; and (5) avoiding carbonate phases containing dolomite or ankerite.

Strontium isotope dating of the Paskenta seep carbonate in California indicates a late Jurassic (Tithonian) age for this deposit. This conflicts with the supposed absence of Jurassic strata in the Great Valley Group, based on zircon dating.

REFERENCES CITED

Aharon, P.; Schwarcz, H. P.; and Roberts, H. H. 1997. Radiometric dating of submarine hydrocarbon seeps in the Gulf of Mexico. Geol. Soc. Am. Bull. 109:568–579.

Berti, M.; Cuzzani, M. G.; Landuzzi, A.; Taviani, M.; Aharon, P.; and Vai, G. B. 1994. Hydrocarbon-derived imprints in olistostromes of the Early Serravallian Marnoso-arenacea Formation, Romagna Apennines (northern Italy). Geo-Mar. Let. 14:192–200.

Bertucci, P. F. 1983. Petrology and provenance of the Stony Creek Formation, northwestern Sacramento Valley, California. In Bertucci, P. F., and Ingersoll, R. V., eds., Guidebook to the Stony Creek Formation, Great Valley Group, Sacramento Valley, California. Pacific Section, Society of Economic Paleontologists and Mineralogists, Los Angeles, p. 1–16.

Bertucci, P. F., and Ingersoll, R. V., eds. 1983. Guidebook to the Stony Creek Formation, Great Valley Group, Sacramento Valley, California. Annual meeting, Pacific Section, Society of Economic Paleontologists and Mineralogists, Los Angeles, 25 p.

Birgel, D.; Himmler, T.; Freiwald, A.; and Peckmann, J. 2008. A new constraint on the antiquity of anaerobic oxidation of methane: Late Pennsylvanian seep limestones from southern Namibia. Geology 36:543–546.

Boetius, A.; Ravenschlag, K.; Schubert, C. J.; Rickert, D.; Widdel, F.; Gieseke, A.; Amann, R.; Jørgensen, B. B.; Witte, U.; and Phannkuche, O. 2000. A marine microbial consortium apparently mediating anaerobic oxidation of methane. Nature 407:623–625.

Buggisch, W., and Krumm, S. 2005. Palaeozoic cold seep carbonates from Europe and North Africa: an integrated isotopic and geochemical approach. Facies 51:566–583.

Campbell, K. A. 2006. Hydrocarbon seep and hydrothermal vent paleoenvironments and paleontology: past developments and future research directions. Palaeogeogr. Palaeoclimatol. Palaeoecol. 232:362–407.

Campbell, K. A., and Bottjer, D. J. 1993. Fossil cold seeps. Nat. Geogr. Res. Explor. 9:326–343.

———. 1995. Brachiopods and chemosymbiotic bivalves in Phanerozoic hydrothermal vent and cold seep environments. Geology 23:321–324.

Campbell, K. A.; Carlson, C.; and Bottjer, D. J. 1993. Fossil cold seep limestones and associated chemosymbiotic macroinvertebrate faunas, Jurassic-Cretaceous Great Valley Group, California. In Graham, S. A., and Lowe, D. R., eds. Advances in the sedimentary geology of the Great Valley Group, Sacramento Valley, California. Pacific Section, Society of Economic Paleontologists and Mineralogists, Los Angeles, p. 37–50.

Campbell, K. A.; Farmer, J. D.; and Des Marais, D. 2002. Ancient hydrocarbon seeps from the Mesozoic convergent margin of California: carbonate geochemistry, fluids and palaeoenvironments. Geofluids 2:63–94.

Denison, R. E.; Koepnick, R. B.; Fletcher, A.; Howell, M. W.; and Callaway, W. S. 1994. Criteria for the retention of original seawater $^{87}Sr/^{86}Sr$ in ancient shelf limestones. Chem. Geol. 112:131–143.

Faure, G., and Mensing, T. M. 2004. Isotopes: principles and applications (3rd ed.). Chichester, Wiley.

Fernando, A. G. S.; Nishi, H.; Tanabe, K.; Moriya, K.; Iba, Y.; Dodama, K.; Murphy, M. A.; and Okada, H. 2011. Calcareous nannofossil biostratigraphic study of forearc basin sediments: Lower to Upper Cretaceous Budden Canyon Formation (Great Valley Group), northern California, USA. Island Arc 20:346–370.

Gill, F. L.; Harding, I. C.; Little, C. T. S.; and Todd, J. A. 2005. Palaeogene and Neogene cold seep communities in Barbados, Trinidad and Venezuela: an overview. Palaeogeogr. Palaeoclimat. Palaeoecol. 227:191–209.

Goedert, J. L., and Squires, R. L. 1990. Eocene deep-sea communities in localized limestones formed by subduction-related methane seeps, southwestern Washington. Geology 18:1182–1185.

Gradstein, F. M.; Ogg, J. G.; Schmitz, M.; and Ogg, G. 2012. The geologic time scale 2012. Amsterdam, Elsevier, 1176 p.

Greinert, J.; Bohrmann, G.; and Suess, E. 2001. Gas hydrate-associated carbonates and methane-venting at Hydrate Ridge: classification, distribution, and origin of authigenic lithologies. *In* Paull, C. K., and Dillon, W. P., eds. Natural gas hydrates: occurrence, distribution, and detection. Geophys. Monogr., p. 99–113.

Ingersoll, R. V. 1978. Paleogeography and paleotectonics of the late Mesozoic forearc basin of northern and central California. *In* Howell, D. G., and McDougall, K. A., eds. Mesozoic paleogeography of the western United States. Pacific Coast Paleogeography Symposium 2, Pacific Section, Society of Economic Paleontologists and Mineralogists, p. 471–482.

———. 1982. Initiation and evolution of the Great Valley forearc basin of northern and central California, U.S.A. *In* Leggett, J. K., ed. Trench-forearc geology: sedimentation and tectonics on modern and ancient active plate margins. Geol. Soc. Lond. Spec. Publ. 10:459–467.

———. 1983. Petrofacies and provenance of Late Mesozoic forearc basin, northern and central California. Am. Assoc. Petrol. Geol. Bull. 67:1125–1142.

Jenkins, R. G.; Kaim, A.; Little, C. T. S.; Iba, Y.; Tanabe, K.; and Campbell, K. A. 2013. Worldwide distribution of modiomorphid bivalve genus *Caspiconcha* in late Mesozoic hydrocarbon seeps. Acta Palaeontol. Pol. 58: 357–382.

Jones, D. E.; Bailey, E. H.; and Imlay, R. W. 1969. Structural and stratigraphic significance of the *Buchia* zones in the Colyear Springs–Paskenta area, California. U.S. Geol. Surv. Prof. Pap. 647A:1–24.

Kiel, S. 2009. Global hydrocarbon seep carbonate precipitation correlates with deep-water temperatures and eustatic sea-level fluctuations since the late Jurassic. Terra Nova 21:279–284.

Kiel, S.; Campbell, K. A.; Elder, W. P.; and Little, C. T. S. 2008. Jurassic and Cretaceous gastropods from hydrocarbon-seeps in forearc basin and accretionary prism settings, California. Acta Palaeontol. Pol. 53:679–703.

Kiel, S., and Little, C. T. S. 2006. Cold seep mollusks are older than the general marine mollusk fauna. Science 313:1429–1431.

Kiel, S., and Peckmann, J. 2007. Chemosymbiotic bivalves and stable carbon isotopes indicate hydrocarbon seepage at four unusual Cenozoic fossil localities. Lethaia 40:345–357.

Kiel, S.; Wiese, F.; and Titus, A. L. 2012. Shallow-water methane-seep faunas in the Cenomanian Western Interior Seaway: no evidence for onshore-offshore adaptations to deep-sea vents. Geology 40:839–842.

Lear, C. H.; Elderfield, H.; and Wilson, P. A. 2000. Cenozoic deep-sea temperatures and global ice volumes from Mg/Ca in benthic foraminiferal calcite. Science 287:269–272.

Levin, L. A. 2005. Ecology of cold seep sediments: interactions of fauna with flow, chemistry and microbes. Oceanogr. Mar. Biol. 43:1–46.

Little, C. T. S., and Vrijenhoek, R. C. 2003. Are hydrothermal vent animals living fossils? Trends Ecol. Evol. 18:582–588.

McArthur, J. M.; Howarth, R. J.; and Shields, G. A. 2012. Strontium isotope stratigraphy. *In* Gradstein, F. M.; Ogg, J. G.; Schmitz, M.; and Ogg, G., eds. The geologic time scale 2012. Amsterdam, Elsevier, p. 127–144.

Murphy, M. A.; Rodda, P. U.; and Morton, D. M. 1969. Geology of the Ono quadrangle, Shasta and Tehama counties, California. Calif. Dep. Nat. Resour. Div. Mines State Min. Rep. 192:1–28.

Newman, W. A. 1985. The abyssal hydrothermal vent fauna: a glimpse of antiquity? Bull. Biol. Soc. Wash. 6:231–242.

Okada, H., and Bukry, D. 1980. Supplementary modification and introduction of code numbers to the low-latitude coccolith biostratigraphic zonation (Bukry, 1973; 1975). Mar. Micropaleontol. 5:321–325.

Olsson, A. A. 1931. Contributions to the Tertiary paleontology of northern Peru. Pt. 4. The Peruvian Oligocene. Bull. Am. Paleontol. 17:97–264.

Paull, C. K.; Chanton, J. P.; Martens, C. S.; Fullagar, P. D.; Neumann, A. C.; and Coston, J. A. 1991. Seawater circulation through the flank of the Florida platform: evidence and implications. Mar. Geol. 102:265–279.

Paull, C. K.; Hecker, B.; Commeau, R.; Freeman-Lynde, R. P.; Neumann, C.; Corso, W. P.; Golubic, S.; Hook, J. E.; Sikes, E.; and Curray, J. 1984. Biological communities at the Florida Escarpment resemble hydrothermal vent taxa. Science 226:965–967.

Peckmann, J.; Birgel, D.; and Kiel, S. 2009. Molecular fossils reveal fluid composition and flow intensity at a Cretaceous seep. Geology 37:847–850.

Peckmann, J.; Reimer, A.; Luth, U.; Luth, C.; Hansen, B. T.; Heinicke, C.; Hoefs, J.; and Reitner, J. 2001. Methane-derived carbonates and authigenic pyrite from the northwestern Black Sea. Mar. Geol. 177:129–150.

Peckmann, J., and Thiel, V. 2004. Carbon cycling at ancient methane-seeps. Chem. Geol. 205:443–467.

Surpless, K. D.; Graham, S. A.; Covault, J. A.; and Wooden, J. L. 2006. Does the Great Valley Group contain Jurassic strata? reevaluation of the age and early evolution of a classic forearc basin. Geology 34:21–24.

Veizer, J. 1989. Strontium isotopes in seawater through time. Annu. Rev. Earth Planet. Sci. 17:141–167.

Veizer, J.; Ala, D.; Azmy, K.; Bruckschen, P.; Buhl, D.; Bruhn, F.; Carden, G. A. F.; et al. 1999. $^{87}Sr/^{86}Sr$, ^{13}C and ^{18}O evolution of Phanerozoic seawater. Chem. Geol. 161:59–88.

Vrijenhoek, R. C. 2013. On the instability and evolutionary age of deep-sea chemosynthetic communities. Deep-Sea Res. Pt. II 92:189–200.

Wortmann, U. G., and Paytan, A. 2012. Rapid variability of seawater chemistry over the past 130 million years. Science 337:334–336.

Wright, J. E., and Wyld, S. J. 2007. Alternative tectonic model for Late Jurassic through Early Cretaceous evolution of the Great Valley Group, California. Geol. Soc. Am. Spec. Pap. 419:81–95.